THE ASTRONOMICAL JOURNAL VOLUME 81, NUMBER 10 OCTOBER 1976

Surface photometry of Virgo cluster galaxies: Barred galaxies

George F. Benedict
Department of Astronomy, University of Texas, Austin, Texas
(Received 28 June 1976)

Photographic surface photometry in B and V is presented for three barred galaxies in the Virgo cluster; N4548 [SB(rs)b], N4596 [SB0$^+$(r)], and N4608 [SB0°(r)]. Intercomparisons of luminosity and color profiles and standard photometric parameters indicate that for these galaxies: (1) the nuclear component follows the $r^{1/4}$ luminosity law for both B and V, (2) the luminosity profiles along the bar show a characteristic shoulder with a slight fall in $\mu_B - \mu_V$ at the brightest point in the bar, the strength of the effect declining from N4548 to N4608, (3) the integrated bar component is slightly bluer than the nucleus, (4) as the disk, arm, and ring components contribute less to the total luminosity of the system, the contribution of the bar increases as does the equivalent gradient $G(r^*)$.

THIS paper presents two-color (B,V) photometry of the brightest regions of three galaxies in the Virgo cluster classified as barred by de Vaucouleurs and de Vaucouleurs (1964). The galaxies and classifications are N4548 [SB(rs)b], N4596 [SB0$^+$(r)], and N4608 [SB0°(r)].

The photometric characteristics of late-type (SBd-m) barred galaxies have been discussed by de Vaucouleurs and Freeman (1973). Three-color UBV surface photometry of N1300 [SB(rs)bc] has been carried out by Burkhead and Burgess (1973). B surface photometry has been published on the transition stage galaxy N1291 [(R) SB(s) 0 /a] by de Vaucouleurs (1975). The present paper deals with the early-type (SB0) barred galaxies (N4596, N4608) and with a galaxy (N4548) very similar in classification to 1300 [SB(rs)bc].

Information regarding the photometric calibration and notation used within this paper can be found in Benedict (1976). In the following sections similar types of data are presented together for all galaxies to facilitate intercomparisons. Each galaxy will be discussed individually, and finally intercomparisons will be made to determine both dissimilarities among and the general photometric characteristics of this set of barred galaxies.

I. THE DATA

Copies from the original plate material are shown in Plate III (p. 899). Detailed profiles [$\mu_B(r)$ and $\mu_B(r) - \mu_V(r)$] are presented in Fig. 1, average profiles [$\langle\mu_B(r)\rangle$ and $\langle\mu_B(r)\rangle - \langle\mu_V(r)\rangle$] in Fig. 2, and equivalent profiles [$\mu_B(r^*)$ and $\mu_B(r^*) - \mu_V(r^*)$] in Fig. 3. The scale is the same for all galaxies within each figure. Features within and general characteristics of each galaxy will be discussed below. Derived equivalent photometric data and data on axis ratios for each galaxy are given in Tables I–III.

II. DISCUSSION OF INDIVIDUAL GALAXIES

For each galaxy we will first identify the more prominent features in the detailed profiles and then describe trends present in the average and equivalent profiles and the equivalent photometric data. The four main components of these galaxies which are present to a greater or lesser degree are the nucleus, the bar, the disk or lens, and the arms. We would like to derive the photometric characteristics of these components for each galaxy, intercompare these characteristics, and then determine their general behavior for this class of galaxy.

A. N4548

To describe features in the detailed profiles, the following format will be used: profile identification given as direction (e.g., SW—southwest): [probable feature identification, r (arcmin), $\mu_B(r)$, $\mu_B(r) - \mu_V(r)$]. The magnitudes and colors are uncorrected for disk contribution. The features outlined below will generally involve more than one data point and/or be readily identifiable with structure visible in Plate III.

The detailed profiles for N4548 are presented in Fig. 1(a). The major axis (axis perpendicular to the bar) has been determined to be at p.a. = 156°. Probable identifications follow. SE: (knot in arm, 1.4, 22.6, +0.6), (spiral arm, 1.69, 22.7, +0.75), (dust lane, 1.9, 23.2, +1.0). NW: (inner ring, 0.5, 22.4, +0.8), (dust lane, 0.95, 23.4, +1.0), (spiral arm, 1.25, 23.1, +0.9). NE: (condensation in bar, 0.6, 21.5, +0.8), (spiral arm, 1.0, 22.4, +0.9). SW: (condensation in bar, 0.6, 21.5, +0.9), (knot in spiral arm, 1.0, 22.1, +0.6), (outer arm, 1.4, 23.3, +0.8). The feature at r = 1.75 arcmin to the NW is a field star. The colors of these features are uncorrected for the contribution of the disk, and are quite similar to the uncorrected colors found by Burkhead and Burgess (1973) for similar features in N1300.

The average major and minor axes are given in Fig. 2. These data along with the detailed profiles confirm the very red nuclear color first noticed by Tifft (1969) who classified this galaxy Sr3. Next note that the bar system is extremely symmetrical. The bar condensations, occurring very nearly at the same radial distance from the center, have not been smeared out very much by the averaging process. The bar in the region $0.29 \leq r \leq 0.86$

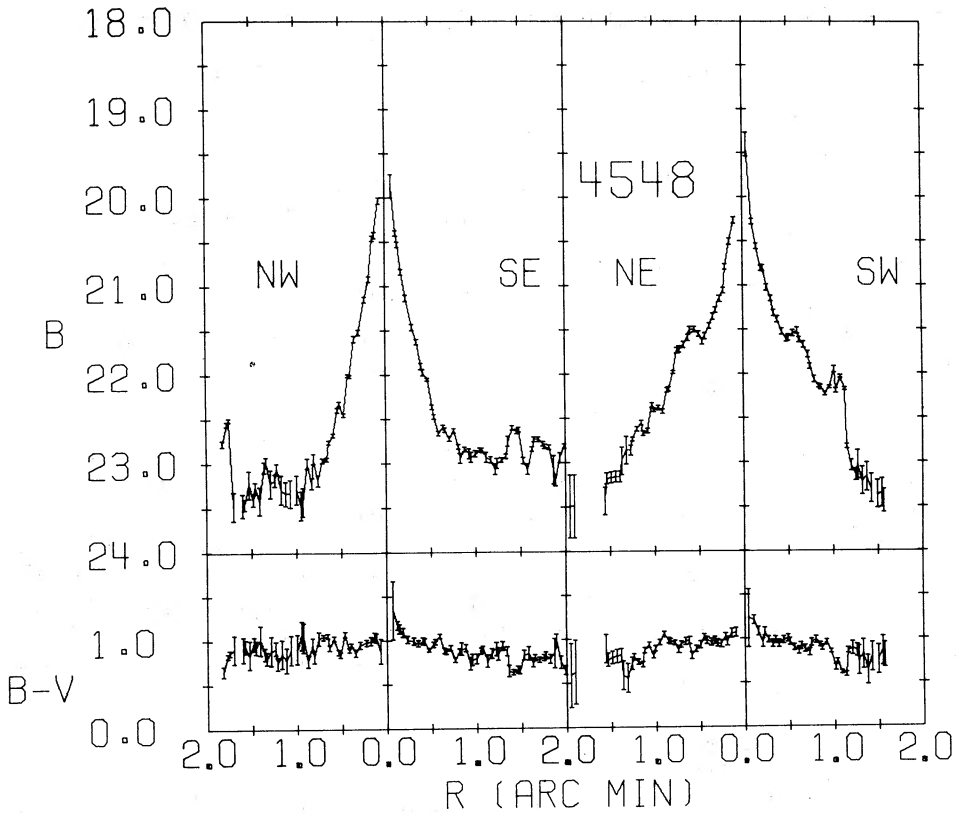

FIG. 1(a). Detailed luminosity and color profiles for N4548. Plotted are $\mu_B(=B)$ and $\mu_B - \mu_V$ $(=B-V)$ within an equivalent aperture of diameter 7 arcsec at the given radial distance from the center of the galaxy in the given directions (SW = southwest, etc.)

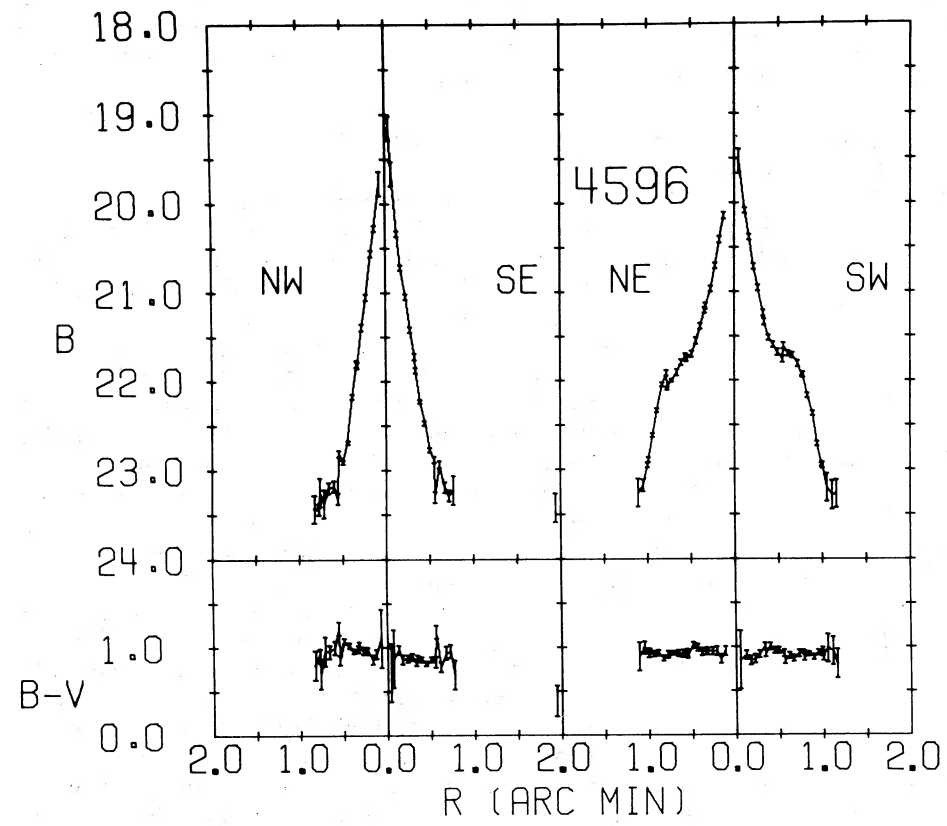

FIG. 1(b). Detailed luminosity and color profiles for N4596. Plotted are $\mu_B(=B)$ and $\mu_B - \mu_V$ $(=B-V)$ within an equivalent aperture of diameter 7 arcsec at the given radial distance from the center of the galaxy in the given directions (SW = southwest, etc.)

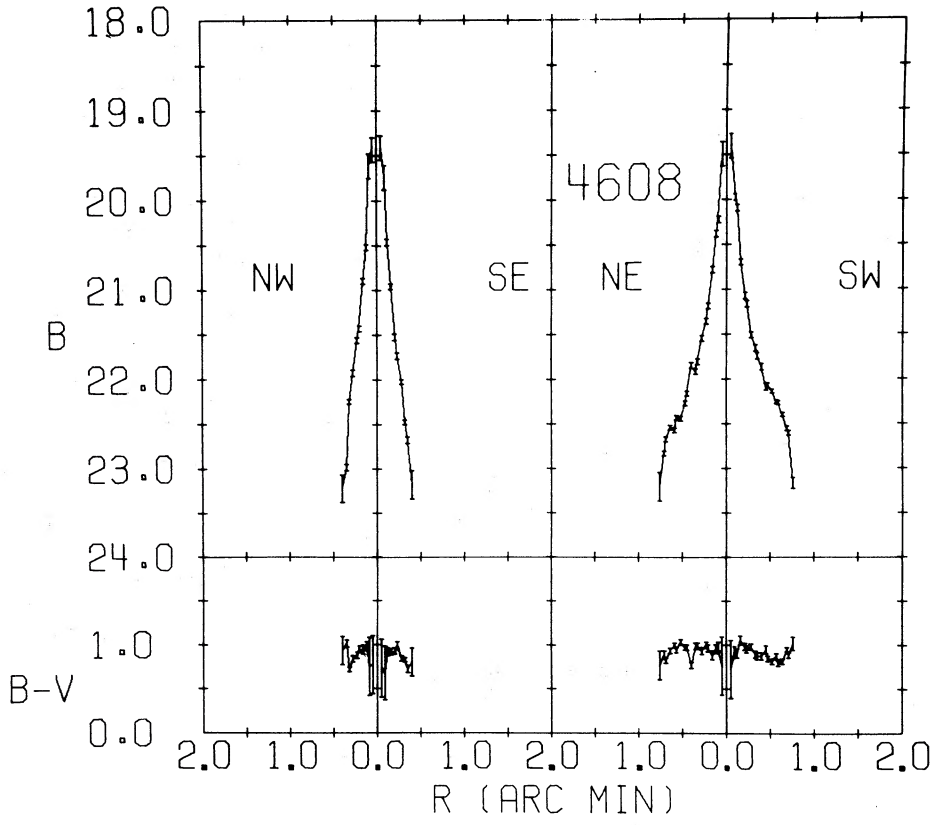

FIG. 1(c). Detailed luminosity and color profiles for N4608. Plotted are $\mu_B(=B)$ and $\mu_B - \mu_V$ $(=B - V)$ within an equivalent aperture of diameter 7 arcsec at the given radial distance from the center of the galaxy in the given directions (SW = southwest, etc.)

arcmin exhibits very little color variation except for perhaps a slight blueing at the condensations. The region of the galaxy along the major axis between the nucleus and the arms ($0.9 \leq r \leq 1.25$ arcmin) exhibits an almost constant brightness, $\mu_B = 23.1$ and color, $\mu_B - \mu_V = +0.8$. The lack of a gradient in this region argues that we are not seeing the disk component. The color is similar to the spiral arms outside of H II regions (for example, the outer arm at $r = 1.4$ arcmin to the SW). Thus, it is probable that this region contains arm material. The lack of any linear features in the average profile plot makes the determination of exponential disk parameters (Freeman 1970) very difficult. If the $\langle\mu\rangle$ values for the axis perpendicular to the bar are plotted versus $r^{1/4}$, we find linear relationships indicative of a spherical component (e.g., de Vaucouleurs 1975) for $\langle\mu_B\rangle$ <23.0 and $\langle\mu_V\rangle$ <22.0. For N4548 these relationships are $\langle\mu_B\rangle = 7.32\ (r^{1/4}) + 16.14$ and $\langle\mu_V\rangle = 7.80\ (r^{1/4}) + 14.72$. Little weight is given the innermost points since the average profiles have not been corrected for seeing effects.

The equivalent surface magnitude and color profiles [Fig. 3(a)] show that the central reddening is produced by a component less luminous than the brightest material in the nuclear region, possibly dust. The magnitude drops steeply, then flattens out in response to the presence of the arms while the color profile exhibits a minimum at $r^* = 0.55$ arcmin due to the brighter component of the spiral arms and the bar condensations [see Fig. 1(a)] and another minimum at $r^* = 1.4$ arcmin due to fainter arm material. A point at $r^* = 2.30$ not plotted but tabulated in Table I shows the equivalent $B - V$ rising abruptly. If the linearity of the data for $\mu_B(r^*) > 22.0$ is taken to be an indication of an exponential disk, we can fit a straight line (giving one-half weight to the point at $\mu_B = 24.0$; see Sec. III for explanation), and derive the gradients $G(r^*)$ and intercepts $\mu(r^* = 0)$ shown in Table V.

Equivalent photometric data along with effective radii, concentration indices, and axis ratio data are presented in Table I. These equivalent photometric data can be used to estimate the relative contributions to the total luminosity of the nucleus, the bar, and the arms. If we plot for the axis containing the bar $\langle\mu_B\rangle$ vs $r^{1/4}$, we find that at $b = 0.35$ arcmin the profile is no longer linear. We can conclude that beyond $b = 0.35$ arcmin ($r^* = 0.31$ arcmin), the nucleus contributes little to the luminosity of the galaxy. Interpolating from Table I [a vs $k(r^*)$] we see that about 10% of the total B luminosity is produced by the nucleus, i.e., by material within $r^* \leq 0.31$ arcmin. The nucleus has an integrated B magnitude and color $[B] = 13.15$ and $[B - V] = +1.02$. From Plate III (p. 899) and Fig. 1(a) the bar is seen to end at $b = 0.86$ arcmin or $r^* = 0.63$ arcmin. Interpolating from Table I, 22% of the B luminosity is produced by the nucleus and the bar, or 12% by the bar alone. For this bar material

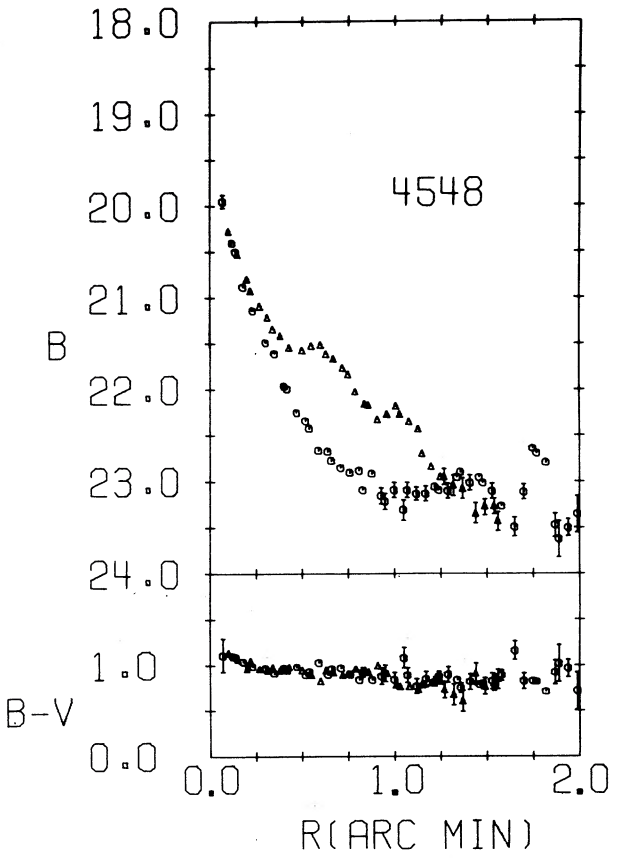

FIG. 2(a). Mean luminosity and color profiles for N4548. Northeast–southwest axis (Δ) and northwest–southeast axis (0), $\langle \mu_B(r) \rangle = (B)$ and $\langle \mu_B(r) - \mu_V(r) \rangle = (B - V)$.

$[B] = 12.95$ and $[B - V] = 0.90$. The remainder of the B luminosity for $\mu_B \leq 24.0$ (55%) is produced by the arms and disk of the galaxy. For this material $[B] = 11.29$ and $[B - V] = +0.82$.

B. N4596

Photographs of N4596 are shown in Plate III. The detailed profiles are presented in Fig. 1(b). The position angle of the major axis (axis containing the bar) was determined to be at p.a. = 76°. The detailed profiles exhibit few variations. SW: (condensation in bar, 0.7, 21.75, +0.95); NE: (condensation in bar, 0.65, 21.8, +0.9); SE + NW: (disk, 0.6, 23.2, +1.0).

The average profiles are found in Fig. 2(b). The entire galaxy has very little color variation from the nuclear value $\mu_B - \mu_V = +1.0$. The bar enhancements have been averaged into a shoulder. The disk component is becoming visible at $r > 1.0$ arcmin on the major axis and $r > 0.5$ arcmin on the minor axis but there are too few points with which to derive disk parameters of the type described by Freeman (1970). The minor-axis average luminosity profiles are linear functions of $r^{1/4}$, the relationships being $\langle \mu_B \rangle = 8.81\ (r^{1/4}) + 15.01$ and $\langle \mu_V \rangle = 8.93\ (r^{1/4}) + 14.02$. The linearity holds for $\langle \mu_B \rangle < 24.0$ and $\langle \mu_V \rangle < 23.0$.

Equivalent photometric data for N4596 are presented in Table II. It is found that the $\langle \mu_B \rangle$ vs $r^{1/4}$ profile for the NE–SW axis (the axis containing the bar) departs from linearity at $a = 0.52$ arcmin or $r^* = 0.39$ arcmin. From Table II we see that 39% of the B luminosity is emitted by the spheroidal component. The integrated magnitude and color of the nucleus of N4596 are $[B] = 12.78$ and $[B - V] = +0.91$. From Fig. 2(b) the bar is seen to decrease in brightness rapidly at $a = 0.97$ arcmin ($r^* = 0.72$ arcmin). Interpolating from Table II [a vs $k(r^*)$] we see that 64% of the total B luminosity is emitted by material within $a = 0.97$ arcmin, and thus the bar alone contributes 25%. The integrated magnitude and color of the bar are $[B] = 13.24$ and $[B - V] = +0.85$. The disk and arms outside $a > 0.97$ arcmin down to $\mu_B = 24.0$ have $[B] = 13.50$ and $[B - V] = +0.79$.

The equivalent surface magnitude and color index data tabulated in Table II are plotted in Fig. 3(b). The color index is, with some scatter, a monotonically decreasing function of r^* except for the abrupt rise at $r^* = 1.17$ arcmin. Since we have determined that the bar

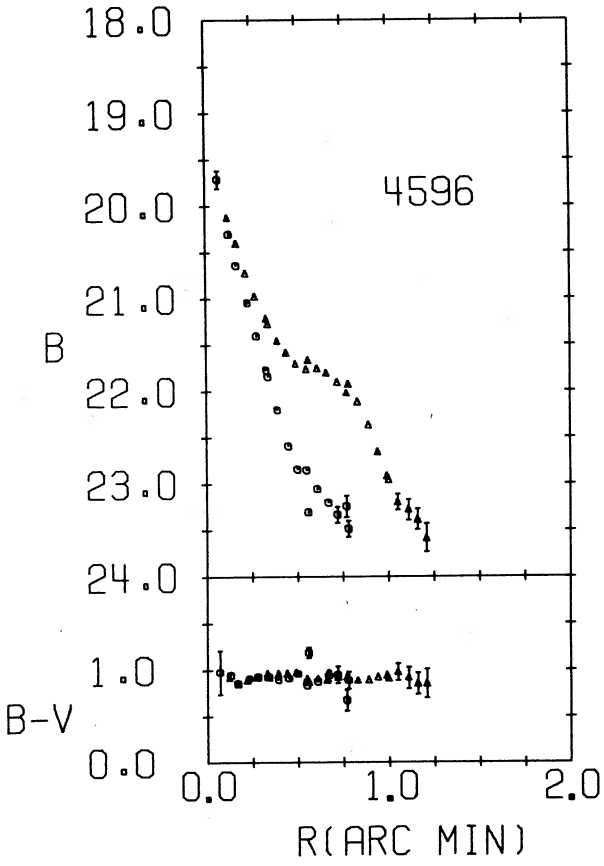

FIG. 2(b). Mean luminosity and color profiles for N4596. Northeast–southwest axis (Δ) and northwest–southeast axis (0), $\langle \mu_B(r) \rangle = (B)$ and $\langle \mu_B(r) - \mu_V(r) \rangle = (B - V)$.

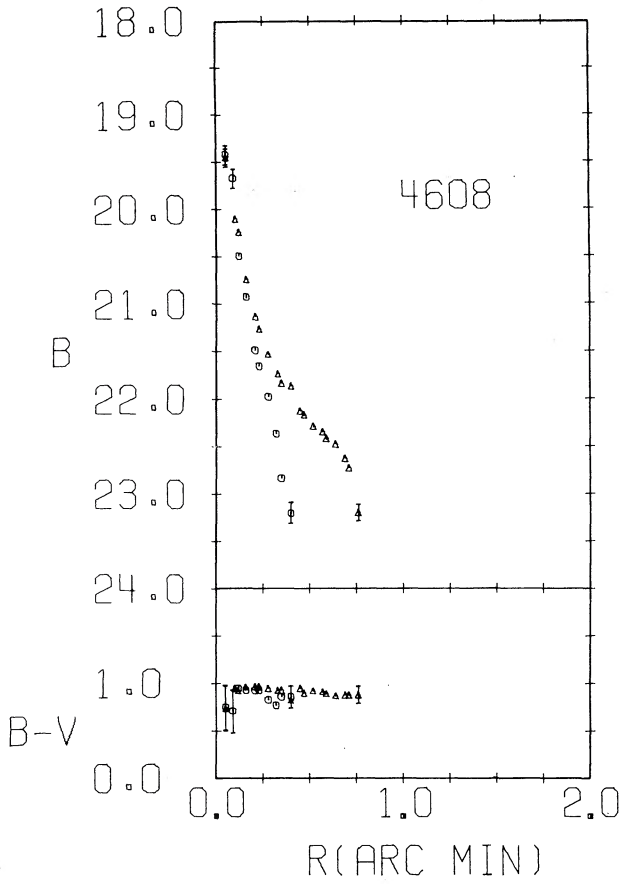

FIG. 2(c). Mean luminosity and color profiles for N4608. Northeast–southwest axis (Δ) and northwest–southeast axis (0), $\langle \mu_B(r) \rangle = (B)$ and $\langle \mu_B(r) - \mu_V(r) \rangle = (B - V)$.

does not continue to contribute to the luminosity of the system for $r^* > 0.72$ arcmin, the surface magnitude data for $\mu_B(r^*) \geq 23.0$ must be due to the disk component of the galaxy. Again giving the data at $\mu_B(r^*) = 24.0$ half-weight we derive the gradients and intercepts tabulated in Table V by fitting a straight line to the data for $\mu_B(r^*) \geq 23.0$.

C. N4608

Reproductions of the original plate material for N4608 are given in Plate III, and the detailed profiles shown in Fig. 1(c). The position angle of the major axis, the axis containing the bar, is p.a. = 28° and labeled NE and SW in Fig. 1(c). There are no significant detailed features evident. The presence of the bar causes the shoulders in the NE and SW profiles.

The average profiles are shown in Fig. 2(c). The shoulder due to the bar is clearly seen. There is a very faint ($\langle \mu_B \rangle > 23.5$) ring around this galaxy with a diameter about equal to the length of the bar. The nucleus of N4608 has an average $\mu_B - \mu_V = 0.95$ until the very center is reached where the color becomes bluer, although since the error is on the order of 0.5 mag in the color, little weight should be attached to this result. There is no hint of the ring or of a disk component in the average profiles. The nucleus obeys the $r^{1/4}$ luminosity relationship along the averaged minor (NW–SE) axis, with $\langle \mu_B \rangle = 12.68\ (r^{1/4}) + 12.85$ and $\langle \mu_V \rangle = 12.81\ (r^{1/4}) + 11.90$, for $\langle \mu_B \rangle < 23.0$ and $\langle \mu_V \rangle < 22.5$.

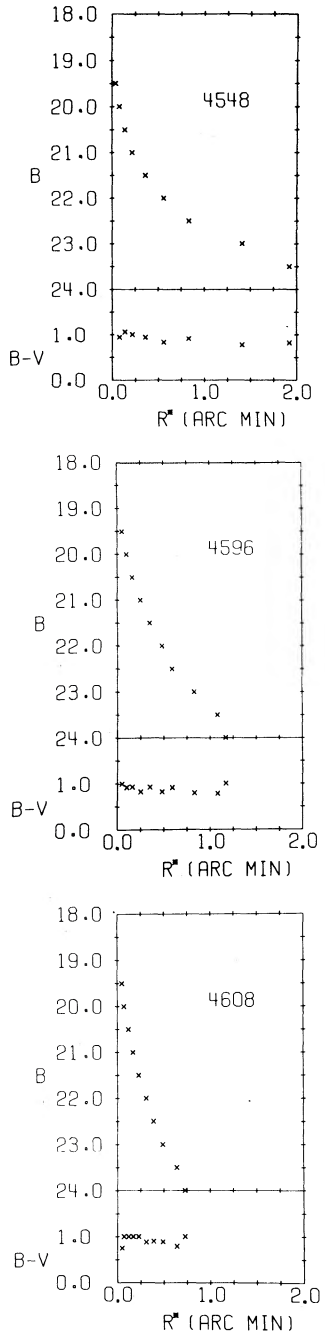

FIG. 3. Equivalent luminosity and color profiles for N4548, N4596, and N4608. Plotted are $\mu_B(r^*) = (B)$ and $[\mu_B(r^*) - \mu_V(r^*)] = (B - V)$.

TABLE I. Equivalent photometric data for NGC 4548.

μ_B	μ_{B-V}	ΣL	$k(r^*)$	r^*	$[B]$	$[B-V]$	ρ^*	$\log J$	α	a	b/a	b
19.5		0.41	0.01	0.04	15.94		0.03					
20.0	0.94	0.98	0.02	0.08	14.98	1.22	0.06	1.21	0.09	0.09	1.00	0.09
20.5	1.06	2.00	0.04	0.14	14.21	1.15	0.10	1.01	0.13	0.14	1.08	0.15
21.0	1.00	3.68	0.07	0.22	13.55	1.05	0.15	0.81	0.20	0.21	1.14	0.24
21.5	0.94	6.41	0.12	0.36	12.94	1.01	0.25	0.61	0.30	0.31	1.35	0.42
22.0	0.83	10.37	0.20	0.56	12.42	0.97	0.39	0.41	0.41	0.43	1.82	0.78
22.5	0.91	15.46	0.29	0.83	11.99	0.93	0.58	0.21	0.54	0.56	1.96	1.10
23.0	0.77	26.19	0.49	1.41	11.41	0.87	0.98	0.01	0.96	1.00	1.28	1.28
23.5	0.82	35.66	0.67	1.92	11.08	0.85	1.33	−0.19	1.73	1.80	0.81	1.46
24.0	0.99	40.92	0.77	2.30	10.93	0.88	1.60	−0.39				
		L_T = 53.11	1.00		10.65 = $[B]_T$			A = −0.56				
	r_1^* = 0.71				9.80 = $[V]_T$							
	r_e^* = 1.44		a_e = 1.04					$[B]$ (r^*) = 11.39				
	r_3^* = 2.22					$\mu_B(r_e^*)$ = 23.03		$[B-V]$ (r_e^*) = 0.87				
	C_{21}^* = 2.03											
	C_{32}^* = 1.54		major-axis p.a. = 156°									

Equivalent photometric data along with axis ratio information are given in Table III. The spherical component of N4608 is found to be dominant along the major axis out to a = 0.25 arcmin (r^* = 0.21 arcmin), i.e., a plot of $\langle\mu_B(a)\rangle$ vs $r^{1/4}$ deviates from linearity at a = 0.25 arcmin. From Table III we interpolate r^* vs $k(r^*)$ and find that 38% of the integrated B luminosity is nuclear in origin, with $[B]$ = 13.70 and $[B-V]$ = +0.91. From Fig. 2(c) the bar is seen to have very little contribution for $a > 0.71$ arcmin (r^* = 0.46 arcmin). The bar and nucleus contribute 69% of the integrated B luminosity and thus the bar alone contributes 31%. The integrated magnitude and color of the bar are $[B]$ 13.95 and $[B-V]$ = +0.86. The ring and disk down to μ_B = 24.0 contribute 18% of the total B luminosity with $[B]$ = 14.51 and $[B-V]$ = 0.89.

The equivalent surface magnitude and color profiles for N4608 are presented in Fig. 3(c). The color index exhibits some peculiarities: the central blueing, two sections of almost constant color, and finally the outer increase at r^* = 0.73. Arguing for N4608, as for N4548 and N4596, we can assume that the surface magnitude data for $\mu_B(r^*) \geq 23.0$ is generated by the disk and ring component. Fitting a line through these data, assigning weight one-half the faintest data point, we derive the gradients and intercepts listed in Table V.

III. INTERCOMPARISON OF PHOTOMETRIC CHARACTERISTICS

From Figs. 1 and 2, some common properties of the luminosity profiles of these galaxies can be discerned. The most obvious property is that the detailed and average surface magnitude profiles along the bars are characterized by structure in the form of shoulders. The fall in luminosity is interrupted by the presence of the bar. The nucleus and the bar have in general very similar $\mu_B - \mu_V$ values. There is a tendency for the condensations in the bars to be slightly bluer than the average for the entire bar (especially N4548, N4596) but the impression is that the bars have nearly constant or slowly blueing color as a function of radius. Note that as the condensations become less luminous from a maximum in N4548 to a minimum in N4608, the difference between $\mu_B - \mu_V$ of the bar outside the condensations and $\mu_B - \mu_V$ of the condensations becomes smaller. Danby (1965) explains the condensations (or "blobs" as he calls them) as being due to matter circulating around and

TABLE II. Equivalent photometric data for NGC 4596.

μ_B	μ_{B-V}	ΣL	$k(r^*)$	r^*	$[B]$	$[B-V]$	ρ^*	$\log J$	α	a	b/a
19.5	1.00	0.65	0.03	0.05	15.43		0.10	1.07	0.07	0.06	1.00
20.0	0.92	1.50	0.08	0.10	14.52	0.94	0.19	0.87	0.13	0.11	0.91
20.5	0.93	2.80	0.15	0.16	13.84	0.90	0.31	0.67	0.23	0.19	0.87
21.0	0.82	4.78	0.25	0.25	13.26	0.91	0.48	0.47	0.33	0.27	0.82
21.5	0.92	6.79	0.35	0.35	12.88	0.91	0.67	0.27	0.50	0.41	0.71
22.0	0.82	9.09	0.47	0.48	12.56	0.91	0.92	0.07	0.94	0.77	0.48
22.5	0.91	10.84	0.56	0.59	12.37	0.90	1.13	−0.13	1.12	0.92	0.48
23.0	0.79	13.64	0.71	0.83	12.12	0.88	1.60	−0.33	1.23	1.01	0.54
23.5	0.78	16.21	0.84	1.08	11.95	0.87	2.08	−0.53	1.40	1.15	0.61
24.0	1.00	16.96	0.88	1.17	11.89	0.87	2.25	−0.73			
		L_T = 19.25	1.00		11.75 = $[B]_T$			A = −0.56			
	r_1^* = 0.25				10.85 = $[V]_T$			$[B]$ (r_e^*) = 12.49			
	r_e^* = 0.52		a_e = 0.82			$\mu_B(r_e^*)$ = 22.17		$[B-V]$ (r_e^*) = 0.91			
	r_3^* = 0.91										
	C_{21}^* = 2.08										
	C_{32}^* = 1.74		major-axis p.a. = 76°								

TABLE III. Equivalent photometric data for NGC 4608.

μ_B	μ_{B-V}	ΣL	$k(r^*)$	r^*	$[B]$	$[B-V]$	ρ^*	$\log J$	α	a	b/a
19.5	0.75	0.64	0.08	0.05	15.45	0.48	0.17	0.94	0.16	0.06	1.00
20.0	1.00	1.01	0.12	0.07	14.95	0.64	0.24	0.74	0.27	0.10	1.00
20.5	1.00	1.83	0.22	0.12	14.30	0.82	0.41	0.54	0.38	0.14	0.86
21.0	1.00	2.61	0.31	0.17	13.92	0.90	0.59	0.34	0.54	0.20	0.85
21.5	1.00	3.50	0.42	0.23	13.60	0.91	0.79	0.14	0.76	0.28	0.79
22.0	0.88	4.40	0.53	0.31	13.35	0.92	1.07	−0.06	1.16	0.43	0.65
22.5	0.90	5.20	0.63	0.39	13.17	0.91	1.34	−0.26	1.70	0.63	0.52
23.0	0.89	5.97	0.72	0.49	13.02	0.89	1.69	−0.46	2.00	0.74	0.50
23.5	0.79	6.81	0.82	0.64	12.88	0.89	2.21	−0.66	2.16	0.80	0.56
24.0	1.00	7.25	0.87	0.73	12.81	0.89	2.52	−0.86			
		$L_T = 8.31$	1.00		$12.66 = [B]_T$			$A = -0.56$			
	$r_1^* = 0.14$				$11.77 = [V]_T$			$[B]\ (r_e^*) = 13.41$			
	$r_2^* = 0.29$		$a_e = 0.37$		$\mu_B(r_e^*) = 21.86$			$[B-V]\ (r_e^*) = 0.91$			
	$r_3^* = 0.54$										
	$C_{21}^* = 2.07$										
	$C_{32}^* = 1.86$		major-axis p.a. = 28°								

through stable points just outside the ends of a Jacobi ellipsoid formed by the bar and the nucleus. The decrease in $\mu_B - \mu_V$ may indicate a low but significant level of star formation resulting from the entrapment of material as discussed by Danby.

The parameters for the spherical components of these galaxies derived from the average minor axis data presented in Fig. 2 are compared in Table IV. The units are minutes of arc and magnitude (arcsec)$^{-2}$. In each case the B gradient is shallower than the V. For N4596 the extrapolated central color is consistent with the detailed and average profile photometry. The extrapolated color is redder than the color derived from the detailed and average photometry for both N4548 and N4608.

The equivalent luminosity and color profiles seen in Fig. 3 all share the following characteristics: a steeply falling $\mu_B(r^*)$ for the nuclear region, a less steep slope for the bar, and finally an outer section with the shallowest gradient. The color index data in general show a slow decline from nucleus to disk with an abrupt rise in $\mu_B(r^*) = 24.0$. This latter feature should be assigned low weight, since it occurs at a level where the photometric errors are of the same order of magnitude as the effect. And, since the effect occurs at the same level for each galaxy, this may be a systematic error, not intrinsic to each galaxy. On the other hand, fluctuations in $\mu_B(r^*)$ of this amount are seen in the equivalent profiles of N1313 (de Vaucouleurs 1963a) and N300 (de Vaucouleurs 1962). Further observations will be required to establish the reality of this feature. For the determination of the equivalent gradients discussed below the data at $\mu_B = 24.0$ were assigned one-half weight.

In Table V are collected the gradients (mag/arcmin) and intercepts (mag/arcsec^2) for the equivalent exponential disks of all three galaxies. The gradients are also given in magnitude/kpc assuming a distance to Virgo, $D = 19.5$ Mpc (Sandage and Tammann 1974). In all cases the B gradient is less steep than the V, and the gradients for N4548 are much shallower than for N4596 and N4608. It is interesting to note (Benedict 1976) that for N4321 [SAB(s)bc] the blue gradient is $G(r^*) = 0.97$ (arcmin)$^{-1}$, very nearly equal to that for N4548. [Note that the gradient as given in Table V (Benedict 1976) has an accidental error in sign.]

Tables I–III show some characteristics in common for all three galaxies. The axial ratios b/a are near unity for the nucleus, reach local minimum (or maximum in the case of N4548, since the axis containing the bar is not the major axis of this galaxy) near the end of the bar. This behavior is seen for other barred galaxies, for example, N1313 (de Vaucouleurs 1963a) and N6744 (de Vaucouleurs 1963b). The reduced luminosity profiles, $\log J$ vs $\rho^* - 1$ tabulated in Tables I–III are not plotted for the three galaxies, but do contain linear sections in the regions indicated: N4548, $\rho^* \geq 0.58$; N4596 $\rho^* \geq 0.92$; N4608, $\rho^* \geq 1.07$. In each case we find slopes consistent with $A = -0.56$ with some scatter. The integrated effective B magnitudes $[B]\ (r_e^*)$ are 11.39 (N4548), 12.49 (N4596), and 13.41 (N4608). The in-

TABLE IV. Parameters of spherical component (nucleus). $\langle\mu\rangle$ = slope × $(r^{1/4})$ + intercept.

	S		I	
NGC	B	V	B	V
4548	7.32	7.80	16.14	14.72
4596	8.81	8.93	15.01	14.02
4608	12.68	12.81	12.85	11.90

TABLE V. Equivalent exponential disk parameters.

	$G(r^*)$		$\mu(o)$	
NGC	B	V	B	V
4548	0.98 (arcmin)$^{-1}$	0.97	21.65	20.81
	0.17 (kpc)$^{-1}$	0.17		
4596	2.55	2.21	20.85	20.37
	0.45	0.39		
4608	3.93	3.79	21.05	20.26
	0.69	0.67		

TABLE VI. Percent contribution, integrated magnitude and color of nucleus, bar, and arm/disk components.

NGC		Nucleus	Bar	Arms/disk ($\mu_B \leq 24.0$)
4548	%	10	12	55
	$[B]$	13.15	12.95	11.29
	$[B-V]$	+1.02	+0.90	+0.82
4596	%	39	25	24
	$[B]$	12.78	13.24	13.50
	$[B-V]$	+0.91	+0.86	+0.79
4608	%	38	31	18
	$[B]$	13.70	13.95	14.51
	$[B-V]$	+0.91	+0.86	+0.89

tegrated effective color indices $[B-V]$ (r_e^*), are all quite similar 0.87 (N4548), 0.91 (N4596), and 0.91 (N4608). The concentration indices C_{21}^* show little variation while the index C_{32}^* varies from 1.54 (N4548) to 1.74 (N4596) to 1.86 (N4608), indicating the relatively greater importance of the disk for the first two galaxies.

A concise intercomparison of the relative integrated contributions of the major components of these three galaxies is given in Table VI. In each case the bar is a little bluer than the nucleus. We see that the percent contribution of the bar is very nearly equal to the contribution of the nucleus for all three and that the contribution of the disk, arms, and/or ring decreases from N4548 to N4608 as is shown, also, by the concentration index C^*_{32}. These data show N4548 and N4596 to be an interesting pair. Note that the B luminosity of the outer regions (disk and arms) of N4548 is greater than $[B]_T$ for N4596, (see Table II) but the B luminosity of the nucleus and bar for N4548 is very nearly equal to the B luminosity of the nucleus and bar of N4596. For N4548, bar + nucleus $[B] = 12.29$ and $[B-V] = +1.00$, while for N4596, bar + nucleus $[B] = 12.23$ and $[B-V] = +0.89$, the difference in color being due in part to the abnormally red nucleus of N4548 (Tifft 1969).

IV. SUMMARY

The bars of the galaxies N4548, N4596, and N4608 produce a characteristic shoulder in both the detailed and average luminosity profiles. The brightest parts of the bars tend to be bluer in $B-V$ than the rest of the bar, this effect declining in strength from N4548 to N4608. The nuclei appear to follow an $r^{1/4}$ surface luminosity relationship for both B and V, the gradient $\langle\mu\rangle/r^{1/4}$ increasing from N4548 to N4608. The equivalent luminosity profiles show the disks of these galaxies to have an exponential nature. As the disk contribution increases relative to the nucleus and bar the gradient is seen to decrease. The photometric properties of the nuclei and bars of the pair N4548 and N4596 are quite similar. Perhaps further study of these two could provide information on the conditions favoring the formation of arms for N4548 and inhibiting their formation for N4596.

ACKNOWLEDGMENTS

I would like to thank V. Tsikoudi for helpful discussions, L. Krizan for typing, R. Lazenby for photographic support, C. Hilburn for figures, and NASA contract NAS 8-31459 for support during the preparation of this paper.

[*Note added to proof:* It should be pointed out that the apparent linearities in the μ_B profiles which were attributed to an exponential disk (see Table V) could be due to the summation of the spheroidal component and a flat-lens component as was shown to be the case for N1291 (de Vaucouleurs 1975). If this is the case, the true exponential disk would show up outside the region of the lens, below the magnitude limit of this photometry.

van den Bergh (1976) has proposed a new classification system for galaxies which includes a sequence of anemic spirals. N4548 is classified as an anemic barred spiral [A(B)b II] while N1300 is classified as a normal barred spiral (SBb I). A comparison of Fig. 1(a) with Burkhead and Burgess (1973, Fig. 3) shows, as has been discussed above, that the surface colors of the arms and lens are similar. The only striking difference is in the contrast of the arms relative to the lens ($\Delta m = 0.9$ for N1300: $\Delta m = 0.5$ for N4548). This is just what is expected given the luminosity classifications indicated by van den Bergh. Preliminarily, little difference can be seen in $\mu_B - \mu_v$ to help discriminate between this pair of normal and anemic spiral galaxies.]

REFERENCES

Benedict, G. F. (1976). Astron. J. **81,** 89.
Burkhead, M. S., and Burgess, R. D. (1973). Astron. J. **78,** 606.
Danby, J. M. A. (1965). Astron. J. **70,** 501.
de Vaucouleurs, G. (1962). Astrophys. J. **136,** 107.
de Vaucouleurs, G. (1963a). Astrophys. J. **137,** 720.
de Vaucouleurs, G. (1963b) Astrophys. J. **138,** 934.
de Vaucouleurs, G. (1975). Astrophys. J. Suppl. **29,** 193.
de Vaucouleurs, G., and Freeman, K. C. (1973). Vistas Astron. **14,** 163.
de Vaucouleurs, G., and de Vaucouleurs, A. (1964). *Reference Catalog of Bright Galaxies* (Univ. Texas P., Austin).
Freeman, K. C. (1970). Astrophys. J. **160,** 811.
Sandage, A. R., and Tammann, G. A. (1974). Astrophys. J. **194,** 559.
Tifft, W. G. (1969). Astron. J. **74,** 354.
van den Bergh, S. (1976). Astrophys. J. **206,** 883.

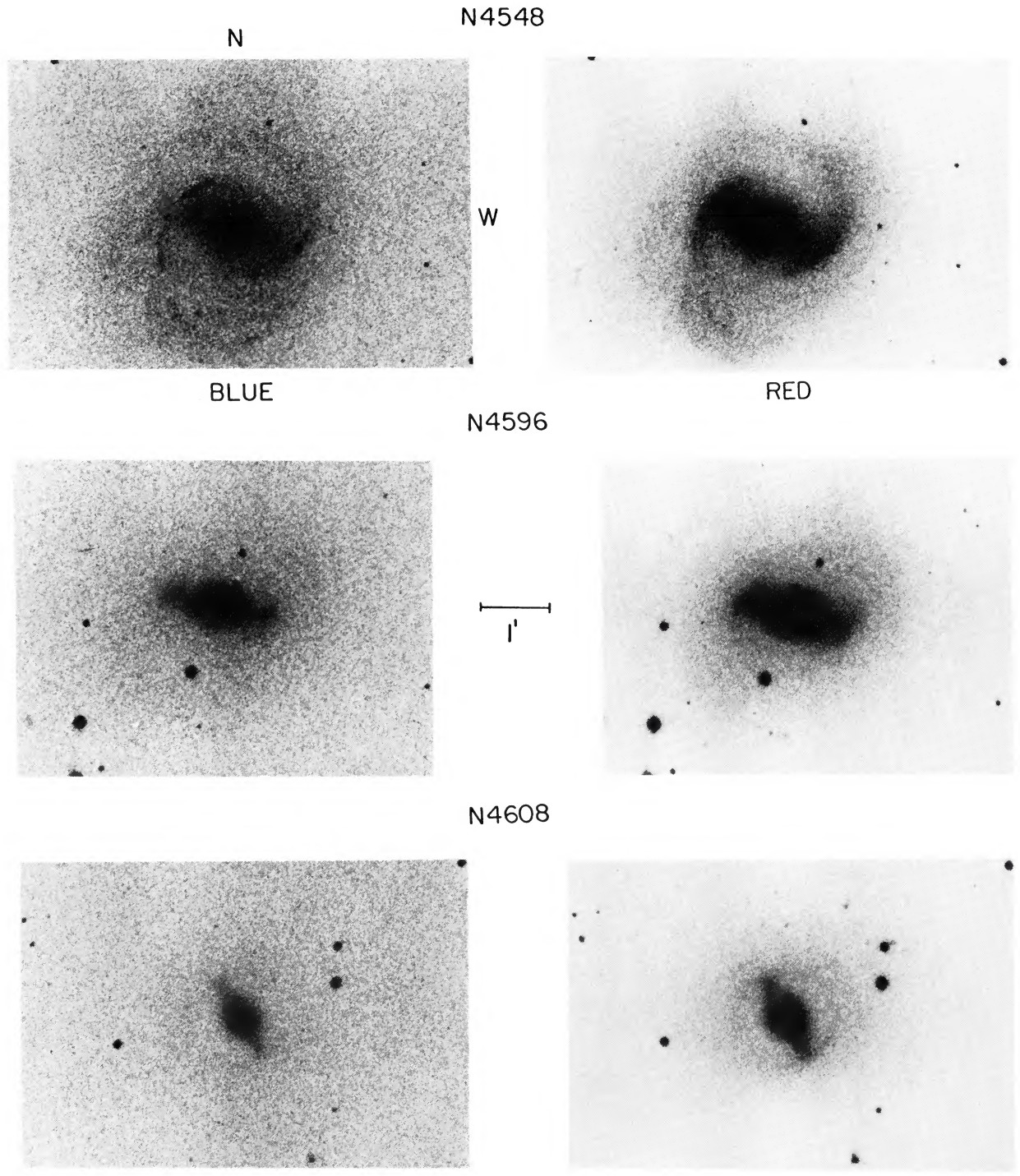

PLATE III (Benedict, p. 799). N4548, N4596, and N4608. Copies from original plate material. Blue (103a-O: exp = 8 min). Red (103a-D +Wr23a: exp = 20 min).